Open access • Journal Article • DOI:10.1103/PHYSREVB.79.134530

Scanning gate microscopy measurements on a superconducting single-electron transistor — Source link

Magdalena Huefner, Christian Albrecht May, S. Kičin, Klaus Ensslin ...+5 more authors

Institutions: Solid State Physics Laboratory, McGill University, École Polytechnique Fédérale de Lausanne, Delft University of Technology

Published on: 29 Apr 2009 - Physical Review B (American Physical Society)

Topics: Scanning gate microscopy, Gate dielectric, Gate oxide, Scanning probe microscopy and Coulomb blockade

PHYSICAL REVIEW B **79**, 134530 (2009)

Scanning gate microscopy measurements on a superconducting single-electron transistor

M. Huefner,* C. May, S. Kičin, K. Ensslin, and T. Ihn
Solid State Physics Laboratory, ETH Zürich, 8093 Zürich, Switzerland

M. Hilke
Department of Physics, McGill University, Quebec, Canada H3A 2T8

K. Suter and N. F. de Rooij
Sensors, Actuators and Microsystems Laboratory (SAMLAB), Institute of Microengineering (IMT), Ecole Polytechnique Fédérale de Lausanne (EPFL), Rue Jaquet-Droz 1, CH-2002 Neuchâtel, Switzerland

U. Staufer
Micro and Nano Engineering PME, 3mE, TU Delft, Mekelweg 2, 2628 CD Delft, The Netherlands
(Received 20 November 2008; revised manuscript received 23 February 2009; published 29 April 2009)

We present measurements on a superconducting single-electron transistor (SET) in which the metallic tip of a low-temperature scanning force microscope is used as a movable gate. We characterize the SET through charge stability diagram measurements and compare them to scanning gate measurements taken in the normal conducting and the superconducting states. The tip-induced potential is found to have a rather complex shape. It consists of a gate voltage-dependent part and a part which is independent of gate voltage. Further scanning gate measurements reveal a dependence of the charging energy and the superconducting gap on the tip position and the voltage applied to it. We observe an unexpected correlation between the magnitude of the superconducting gap and the charging energy. The change in E_C can be understood to be due to screening, however the origin of the observed variation in Δ remains to be understood. Simulations of the electrostatic problem are in reasonable agreement with the measured capacitances.

DOI: 10.1103/PhysRevB.79.134530 PACS number(s): 73.21.La, 73.23.Hk, 74.50.+r

I. INTRODUCTION

A broad variety of quantum dots has been investigated over the last years. Even though fabrication and control of these zero-dimensional systems are rather complex, it is by now established to control individual electrons on semiconductor quantum dots.[1,2] Most transport experiments measure macroscopic currents and voltages. These quantities contain spatial information of wave functions only in an indirect way. To investigate the local electronic structure of a quantum dot, one needs to take a different approach. An option is scanning probe microscopy, where a metallic tip is used as a movable gate. The tip interacts capacitively with the sample. Since the tip can be moved freely in all three dimensions, data can be acquired that has a certain spatial resolution. Measurements employing this technique have been performed on various semiconductor nanostructures[3–8] including quantum dots.[9–12]

In semiconductor quantum dots there are two dominant energy scales, namely, the charging energy, which depends on the capacitance and therefore the geometry of the dot and its gate electrodes including the tip, and the single-particle level spacing arising from the quantum-mechanical confinement of the system. It is a challenge to disentangle these two energy scales with a scanning gate experiment and to extract spatial information about individual quantum states.[13,14] As shown in Ref. 13 the tip-induced potential in the plane of the two-dimensional electron gas in which the quantum dot is formed can be complex and may consist of two additive parts, of which only one depends on the voltage applied to the tip. It was shown that it is possible to observe distinct features related to a specific quantum state when performing scanning gate measurements on a semiconductor quantum dot. It remained, however, an open question if these features were related to the dissimilar wave functions of the different quantum states.

In metallic single-electron transistors (SETs) the single-particle level spacing is orders of magnitude too small for being observable.[15] For superconducting single-electron transistors new energy scales enter the problem, namely, the energy gap Δ of the superconductor and the Josephson energy E_J.

Here we present scanning gate measurements performed on a superconducting SET. Spatial images of the differential conductance give insight into the interaction potential between the tip and the electrons in the SET. We investigate in detail how the charging energy as well the superconducting gap of the SET island depend on tip position and the voltage applied to the tip.

II. SETUP

The aluminum SET is fabricated on a silicon dioxide substrate employing the method of shadow evaporation.[16,17] Between the two evaporation steps the sample is exposed to oxygen in order to form the tunnel barriers between the SET and the leads. Figure 1(a) shows a scanning electron microscope picture of such a SET. The lateral dimensions of the SET island are about $60\times40\ \text{nm}^2$. The thickness of the Al is about 20 nm, the thickness of the oxide barrier about 1 nm. The SET island is connected to source S and drain D via

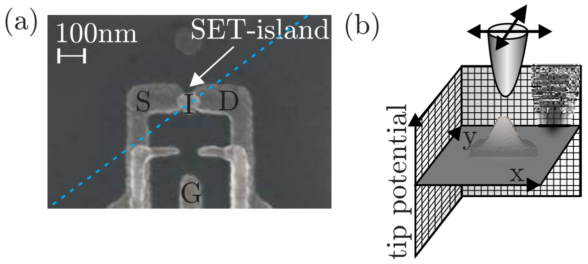

FIG. 1. (Color online) (a) Topography of the SET, where *S* is the source, *D* is the drain, *G* marks the gate, and *I* the SET island. (b) Schematic of the local potential induced by the SFM tip.

tunnel barriers of an area of approximately 20×40 nm^2. A gate *G* is located about 300 nm away from the SET.

The measurements are carried out with a scanning force microscope (SFM) operating in a ^{3}He cryostat with a base temperature of around 300 mK. The scanning sensor consists of an electrochemically etched PtIr tip with an initial radius of 50 nm, mounted on a piezoelectric tuning fork.[18] This tip induces a local electrostatic potential (called tip-induced potential or tip potential for simplicity) in the sample below as schematically shown in Fig. 1(b). The magnitude of the potential can be changed by applying a voltage V_T to the tip or changing the tip-sample separation in z direction. The scanning gate measurements shown in this paper are carried out by scanning the tip at a constant height $z=50$ nm above the sample surface and recording the differential conductance of the SET as a function of the tip position. No current flows from the tip to the sample due to the vacuum gap of 50 nm between them. The system can be kept at base temperature for up to 3 days. The sample can be measured up to a couple of days without visible charge rearrangements. Due to a vibration reduced setup we can expect the distance between the tip and the sample to be very stable. Standard lock-in techniques are used to measure the conductance of the SET.

III. TRANSPORT MEASUREMENTS

In order to characterize the SET before performing scanning gate experiments, measurements of the differential conductance (dI/dV_{SD}) as a function of the source-drain voltage V_{SD} and the gate voltage V_G are carried out. Such charge stability diagrams (Coulomb blockade diamonds) give insight into the transport processes that contribute to the current flow.[19–22] They also contain information about the charging energy E_C, the superconducting gap Δ, as well as the capacitances involved.

While Coulomb blockade diamonds are recorded, the SFM tip is kept at a constant position 70 nm above the SET and the sample is kept at a temperature around 700 mK, well below the critical temperature T_C of aluminum which is around 1.2 K.[23] In order to measure a Coulomb blockade diamond in the normal conducting state a magnetic field of 0.5 T is applied.

Figures 2(a) and 2(b) show the dI/dV_{SD} data of the SET in the normal conducting state measured at finite magnetic field and plotted on a logarithmic scale in (a) and a linear scale in (b). Figures 2(c) and 2(d) show the corresponding Coulomb blockade diamonds of the SET in the superconducting state at $B=0$ T.

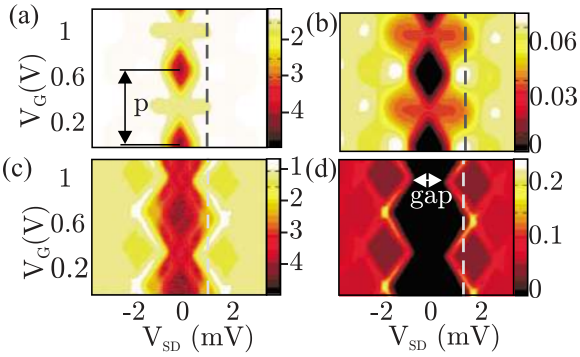

FIG. 2. (Color online) (a) Coulomb blockade diamond of the SET in the normal conducting state recorded at a magnetic field $B=0.5$ T and a temperature $T=700$ mK. Color bar shows the differential conductance $\log_{10}(dI/dV_{SD})$ with the differential conductance dI/dV_{SD} in units of e^2/h plotted on logarithmic scale, whereas (b) shows the same Coulomb blockade diamond plotted on a linear scale. Color bar shows $dI/dV_{SD}(e^2/h)$. (c) Coulomb blockade diamond of the SET in the superconducting state recorded at $B=0$ T and $T=700$ mK, plotted on logarithmic scale. Color bar shows the value of $\log_{10}(dI/dV_{SD})$ with the differential conductance dI/dV_{SD} in units of e^2/h. (d) The same Coulomb blockade diamond on linear scale. Color bar shows $dI/dV_{SD}(e^2/h)$.

In the dI/dV_{SD} data recorded in the normal conducting state, diamond-shaped regions are visible, where the differential conductance is zero. We can estimate the charging energy E_C from the extent of these Coulomb blockade diamonds in the direction of V_{SD} and find it to be around 1 meV.

Without the external magnetic field we observe that the diamonds do not close any more at zero V_{SD} but we rather observe a gap in V_{SD} direction of about 1.6 mV. This gap as indicated in Fig. 2(d) is a measure of the superconducting gap Δ which is one eighth of this total gap which is about 0.2 meV in our case. This behavior has been reported in numerous publications.[21,24,25]

In order to understand the scanning gate measurements presented later in this paper, it is important to realize that the position of the center of a Coulomb blockade diamond, its extent p along the gate voltage axis [see Fig. 2(a)], as well as E_C are the same in the superconducting and the normal state.

The most pronounced feature in the superconducting diamond is the transition in V_{SD} direction from the almost insulating regime to the conducting regime, where transport is dominated by resonant quasiparticle tunneling. This sharp rise in the current will be referred to as current onset (CO) in the rest of the paper. Due to finite temperature in our setup, we do not expect to see processes such as Andreev reflections or Josephson quasiparticle processes inside the Coulomb blockaded regions as they were observed in other measurements at lower temperatures.[21,25] The Josephson energy E_J can be estimated using $E_J=(\hbar I_C)/(2e)=h\Delta/(8e^2R)$ to be 0.1 μeV, where I_C is the junction critical current and R the tunnel resistance of a single junction. The thermal energy k_BT is about 0.06 meV which is 1–2 orders of magnitude smaller then E_C and Δ. Between each of the relevant energy

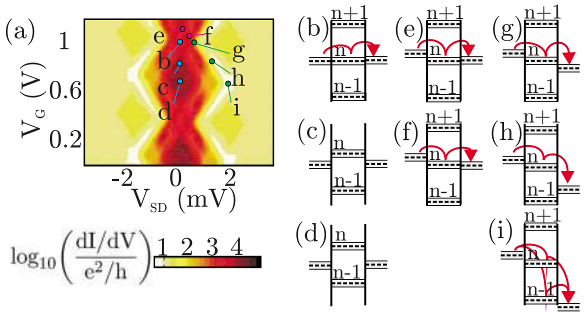

FIG. 3. (Color online) (a) Coulomb diamond of the SET in the superconducting state recorded at $B=0$ T and plotted in logarithmic scale. Columns (b)–(i) show schematics of the energy-level structure to illustrate how electric transport takes place.

scales $E_C > \Delta \gtrsim k_B T \gg E_J$ there is about 1 order of magnitude difference. Since $E_C \gg E_J$ Josephson processes are strongly suppressed and transport is dominated by Coulomb blockade. The thermal energy available in the system is not negligible compared to Δ. Therefore thermally activated quasiparticle tunneling can take place, as seen in Fig. 2(c).

To visualize the relevant transport processes, schematic sketches of the energy-level structure are shown in Fig. 3 for different positions inside the Coulomb blockade diamond. Each sketch consists of the Fermi level of the source and drain to the left and right as well as the single levels inside the SET shown in the middle and labeled with $i=n+1, n, n-1$. Gray-shaded intervals represent the superconducting gap Δ. The solid vertical lines represent the tunnel barriers between the island and the leads. At the center of the Coulomb blockade diamond [Fig. 3(d)], all levels are detuned. No energy is available to produce quasiparticle tunneling. When moving to higher gate voltages, the levels in the SET move down [Fig. 3(c)] until one of them becomes resonant with the source and drain levels [Fig. 3(b)]. When moving from this point to finite source-drain voltages [Fig. 3(g)], the source and drain levels shift antisymmetrically compared to the SET level. This shift becomes large enough to allow quasiparticle tunneling at the CO. When moving along the CO to lower V_G [Fig. 3(h)] the source level stays at the same relative position compared to the SET level, while the drain level is shifted further down. At the outermost peak of the CO [Fig. 3(i)] the source and drain levels have been shifted far enough apart that two levels in the SET can contribute to transport. As shown by [Figs. 3(e) and 3(f)] processes inside the Coulomb blockaded region are also possible due to the thermal energy available in the system.

From the period p of $dI(V)/dV_{SD}$ typical values for the gate-island and the tip-island capacitances of 0.3 and 0.6 aF, respectively, are determined. The capacitance of the island C_Σ is derived from E_C using $C_\Sigma = e^2/E_C$. We assume that each of the two junctions has the same capacitance, since the fabrication process and the area are the same. Therefore the junction capacitance can be calculated using $C_{SD}=(C_\Sigma - C_G)/2$. We find it to be around 80 aF. This value is consistent with the capacitance one would expect when approximating the junction capacitance using a simple plate capacitor model with areas of 20×50 nm^2, which is calculated to be 77 aF.

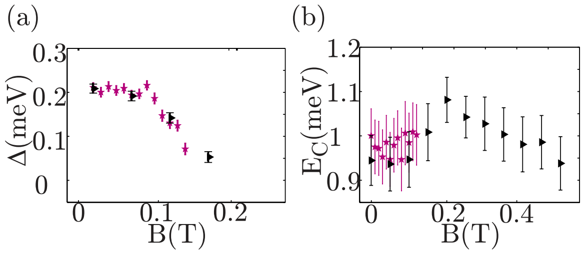

FIG. 4. (Color online) (a) Decay of the superconducting gap vs magnetic field. (b) Change in the charging energy as a function of magnetic field. The two different symbols mark two data sets, taken in different condensation cycles.

Figure 4 shows the dependence of E_C and Δ on the magnetic field. The superconducting gap Δ reduces until the system reaches the normal conducting state around 0.2 T [Fig. 4(a)]. However, the charging energy E_C remains essentially constant for both the superconducting and the normal conducting states as seen in Fig. 4(b).

The exact evaluation routine to derive those quantities from the Coulomb blockade measurements will be described later on. However, the evaluation routine is slightly changed when reaching a magnetic field of $B=0.2$ T, as the employed model only works for the superconducting state. Above $B=0.2$ T the superconducting gap is approximately zero and only the charging energy was deduced from the Coulomb blockade diamonds. As can be seen in Fig. 4(b), when changing the evaluation procedure, E_C rises slightly and then decreases indicating that the superconducting gap might not have reached completely zero below $B=0.4$ T. However for all data points below $B=0.2$ T this analysis shows that the charging energy is little if not at all influenced by the magnetic field, whereas the superconducting gap clearly is.

IV. SCANNING GATE MEASUREMENTS

In the following we present scanning gate measurements of the SET in the normal and superconducting states. Because the SFM tip acts as a movable gate, changing the voltage applied to the tip or changing its position should have a similar effect as changing the voltage applied to the in-plane gate. The voltage applied to the tip was kept constant for one single scan, as was the separation z between sample surface and tip. The influence the tip has on the SET depends on the xy position in the scan frame [Fig. 1(b)].

Figure 5 shows scanning gate measurements taken at two different magnetic fields. Let us start by discussing the SET in the normal conducting state. Figure 5(a) shows a scanning gate image taken at a magnetic field of $B=0.5$ T, $V_T=0$ V, $V_G=0$ V, and $V_{SD}=1.5$ mV, which corresponds to the source-drain voltage marked by the dashed line in Fig. 2(a). We observe concentric ring-shaped features. The island itself is expected to be located at the center of the concentric rings. However, an exact position of the island cannot be given due to the complexity of the tip. The inset shows a cross section through the scanning gate image taken along the dashed line in Fig. 5(a). When looking along the line in Fig. 2(a) we see

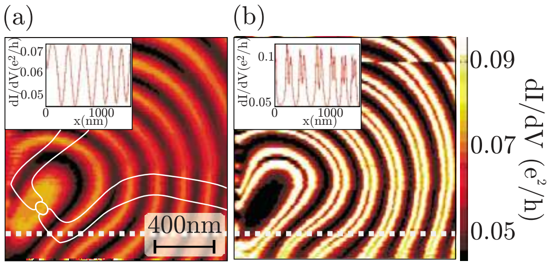

FIG. 5. (Color online) Scanning gate measurements for different magnetic field. The tip-sample distance is around 50 nm, $V_G=0$ V, and $V_{SD}=1.5$ mV. The scanned area is 1.51×1.51 μm^2 (a) at $B=0.5$ T and (b) at $B=0$ T. Insets show cross sections at the position of the gray dotted line. White lines in (a) mark the approximate position of source, drain, and SET of the structure.

regularly spaced Coulomb resonances with a constant period p in V_G direction. For the chosen V_{SD} voltage we do not expect to cut through the Coulomb blockaded regime. However, we expect one maximum in the current in each period p. Furthermore, we find the peak distances to have a monotonic behavior. This can be clearly observed in the inset of Fig. 5(a).

Figure 5(b) shows a scanning gate measurement of the same scan frame as in Fig. 5(a) but in the situation where the SET is in the superconducting state. Since the two measurements have been carried out one right after another and no charge rearrangements were observed, we can assume the SET to be in the same now superconducting state until the clearly visible charge rearrangement in the last quarter of the measurement in the superconducting state takes place. The signature of superconductivity at this source-drain voltage is the splitting of the resonance rings. Every single ring splits up into two when the SET is scanned in the superconducting state. This finding is consistent with the features observed in the Coulomb diamonds. Looking at the dashed line in Fig. 2(d) we can see that for each period p in the superconducting state we expect to cross the line of current onset twice. When looking at the insets in Fig. 5(b) we see a difference in the peak height as compared to the normal conducting scanning gate measurement. This is consistent with the fact that for the normal conducting state we do not reach the regime of total Coulomb blockade for the chosen source-drain voltage, whereas for the superconducting state we cross the line of the current onset. The observations made in these scanning gate measurements are consistent with the Coulomb diamonds discussed before. Since the number of features as well as their spacing is the same for the superconducting and normal conducting state, we know that we can controllably load single electrons onto the SET by scanning the tip.

The noncircular shape of the Coulomb rings is presumably due to a tip shape that is not completely rotationally symmetric around the z axis.[26] This can probably be attributed to the topography scanning carried out before the scanning gate measurement, which led to slight deformations, or the attachment of unwanted particles to the tip. Both effects have been observed before in scanning gate measurements.[26]

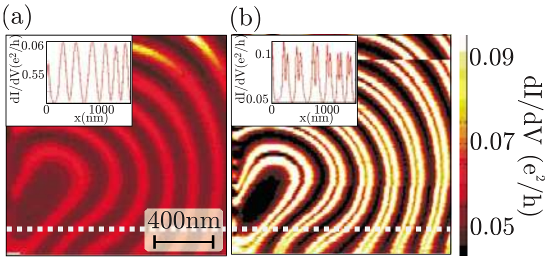

FIG. 6. (Color online) Scanning gate measurements for different temperature. The tip-sample distance is around 50 nm, $V_G=0$ V, and $V_{SD}=1.5$ mV. The scanned area is 1.51×1.51 μm^2 (a) at $T=2$ K and (b) at $T=700$ mK. Insets show cross sections at the position of the gray dotted line. (b) and Fig. 5(b) are identical.

The effect of temperature on the scanning gate measurement is investigated in Fig. 6. We observe that the double rings found in the superconducting state merge into single rings when the temperature is sufficiently high to suppress superconductivity. The position of the rings remains unchanged by this transition. This is in good accordance with the measurement at finite magnetic field. However, the resonances in the normal conducting state are broader due to the higher temperature. Further investigations of the influence of the bias voltage V_{SD} on the scanning gate measurements are shown in the Appendix.

V. TIP-INDUCED POTENTIAL

In order to learn more about the tip-induced potential, a measurement of the differential conductance as a function of V_T is performed while moving the tip along a line across the SET. The approximate position of this trace is shown as a dashed line in Fig. 1. The height z of the tip above the surface was constant at 200 nm. At each of the 1950 steps along this line a trace of the differential conductance as a function of the tip voltage was recorded. Figure 7(a) shows the result of this measurement.

We see how the positions of the Coulomb peaks change when altering the tip position relative to the SET. We observe a concave and a convex part, which means that our tip potential consists of an attractive and a repulsive component. However, there is no tip voltage value in the investigated regime, where the tip does not induce any charge on the SET

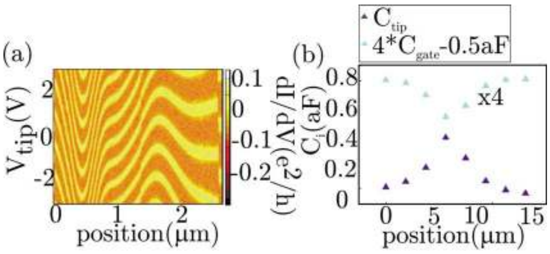

FIG. 7. (Color online) (a) Conductance of the SET vs the voltage applied to the tip along one line over the SET. From this we can see that the tip potential has an attractive and a repulsive part. The tip-sample distance is around 50 nm, $T=700$ mK, $V_{SD}=0$ V, and $B=0$ T. (b) shows the gate and the tip capacitances obtained from different Coulomb diamonds in dependence on the position of the SET.

at all positions along the line. This is in agreement with the observations made previously on semiconductor quantum dots.[27] One would expect to observe a least invasive tip voltage close to the value one estimates from the work-function differences. Contrary to this expectation, we do not find a least invasive voltage here, even though it would be expected at an offset voltage of 1.4 V because of the work-function difference between PtIr ($\phi_{\mathrm{Pt}} \approx 5.6$ eV) and Al ($\phi_{\mathrm{Al}} \approx 4.3$ eV).

The shapes of the single resonance curves are almost identical. This indicates that the shape of the tip-induced potential is independent of the voltage applied to the tip. A change in V_T only changes the offset of this potential, not its shape over the length scale of this measurement. This is the manifestation of a strong contribution to the tip-induced potential which is independent of V_T. It may result from charged debris attached to the tip.[13] The V_T-dependent contribution to the tip-induced voltage becomes visible on larger length scales in the gate and the tip capacitances, as deduced from Coulomb blockade diamond measurements. Figure 7(b) shows C_T and C_G as derived from single Coulomb blockade diamond measurements performed as the tip is positioned on various points along one line across the SET. We observe a smoothly shaped single peak dependence for both capacitances, with a width of several micrometers. The change in C_G is due to the fact that the gate gets shielded from the SET by the presence of the tip. Therefore the change in C_G is much smaller than the change in C_T and inverse in sign to it. However, the change in C_T by 0.4 aF is small compared to the capacitance of the system, which is around 161 aF. It is interesting to note that even though the tip potential looked quite complex at the point of time of this measurement, the capacitances only show a very smooth Gaussian dependence. This confirms that the tip potential is the sum of two independent parts of which only one depends on V_T.

VI. ANALYSIS OF THE TIP-INDUCED POTENTIAL

It has been shown in Ref. 13 that for scanning gate experiments on a semiconductor quantum dot fine structure could be observed that depended on which quantum state the dot was kept. The exact interpretation, however, remained an open question. When performing scanning gate measurements on a metallic SET, we do not expect to see features connected to individual single-particle wave functions since in metals the single-particle energy scale is negligible.

In order to shine further light on this question, two scanning gate measurements are performed where all settings were kept exactly the same, except that the gate voltage was changed by 1 Coulomb diamond period p to reach a different charge state. Figure 8 shows two such scanning gate measurements in (a) and (b). Figure 8(c) shows the difference of those two measurements. We see that some of the rings do overlap as expected. However, in the center the measurement in (a) shows rings with a smaller radius than the measurement in (b), whereas at the outermost rings the opposite seems to be the case. Therefore we have to conclude that a shift in gate voltage by p does not lead to exactly the same scanning gate image. This is contrary to our expectations that the Coulomb rings should overlap completely when carrying out two scanning gate measurements for two different charge states in a metallic SET. We therefore have to conclude that the period depends on the position of the tip, i.e., $p = p(x,y)$.

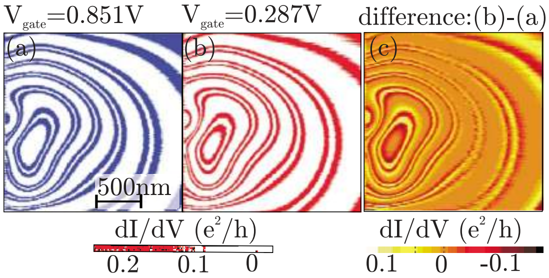

FIG. 8. (Color online) Scanning gate measurement for two different V_{gate} voltages. [Color bar is the same for (a) and (b) shown here only once for simplicity]. (c) shows the difference of those two measurements. One can see that although only one electron was added onto the SET the scanning gate measurement shows a different spacing of the Coulomb rings. The tip-sample distance is around 50 nm, $T = 700$ mK, $V_{SD} = 1.5$ mV, and $B = 0$ T. The scanned area is 2×2 $\mu\mathrm{m}^2$

As a conclusion, we have shown that the influence the tip exerts on the SET during scanning gate measurements is similar to the influence of a planar gate. Although we have a complex tip potential, we are able to control the occupation of the SET island on the level of single electrons. The tip-island capacitance can be changed by about 0.3% of the value of the total capacitance of the island. Furthermore the measurement shown in Fig. 8 reveals that the period p is influenced by the position of the scanning tip.

VII. INVESTIGATION OF THE CHARGING ENERGY

Knowing that the period p and with it the charging energy depends on the SFM tip position, the next open question is how other parameters extracted from the Coulomb diamonds depend on the tip position or voltage. For the first measurement (grid measurement) a grid of 36 tip positions is chosen that covers the scan frame shown in Fig. 8. At each of these 36 positions a Coulomb diamond is recorded and Δ, E_C, C_G, and C_T are extracted. In order to reach a good comparability of these data points all 36 points are measured in the same condensation cycle of the fridge. Because of time constraints the Coulomb blockade diamonds are not recorded with the resolution shown in Fig. 2, but rather reconstructed from V_{SD} sweeps at as few V_G voltages as needed to extract the desired quantities. In order to cover a larger lateral distance the same measurement is carried out for a number of positions distributed along a stretch of 15 μm across the SET (line measurement, see Fig. 1).

Since we also want to investigate the influence of the tip voltage on Δ, E_C, C_G, and C_T, Coulomb blockade diamond measurements are carried out for a constant tip position but changing tip voltages ranging from 0 to 7 V. Two sets of measurements are carried out in different condensation cycles, referred to as V_T data 1 and 2.

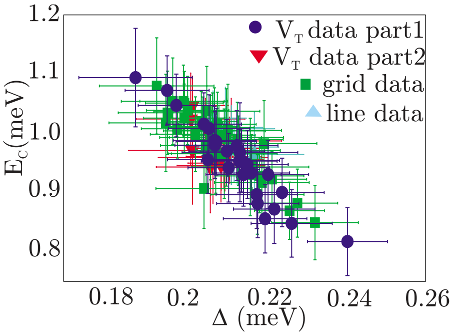

FIG. 9. (Color online) Δ over E_C extracted from Coulomb blockade diamond measurements taken at different lateral tip positions and voltages applied to the tip. The distance of the tip from the surface was kept constant.

The charging energy and the superconducting gap can be read from a Coulomb diamond when the innermost and outermost positions in V_{SD} direction of the CO are known. To determine those positions the COs are fitted linearly from four dI/dV_{SD} versus V_{SD} sweeps (using two sweeps to determine the rising slope and two sweeps to determine the declining slope). As the peak shape of the CO varies, it is not possible to fit all peaks to determine the position of the CO. The CO was rather determined to be positioned at the maximum of each trace. The period $p(x,y)$ of the Coulomb blockade diamonds is determined from a dI/dV_{SD} versus V_G sweep. Assuming this period to be constant over a V_G range of several Coulomb blockade diamonds, the two lines that fit the COs were shifted in V_G direction by p in order to determine the cross sections of the rising and falling slopes of the CO. Those cross sections correspond to 4Δ and $4\Delta+E_C$ in V_{SD}.

Figure 9 shows the most striking result of these measurements. We observe an anticorrelation between E_C and Δ. For different tip positions and voltages neither E_C nor Δ stay constant; they rather vary by about 15% and 20%, respectively. For situations where the charging energy is large (small) the superconducting gap is small (large). However because of the complexity of the tip potential it is impossible to make out a certain spatial trend in this variation. Even though the variation in the superconducting gap Δ is unexpected, the variation in E_C and p itself can be understood, as we will discuss in detail in the next section. We compare the cross sections taken at the minimum and the maximum V_{SD} value of the CO of two Coulomb diamonds, taken at different positions. In Fig. 10, the maximum value of V_{SD} of the CO stays almost the same; the minimum value, however, shifts.

In order to verify that this correlation does not arise from a systematic error, such as the fact that the CO does not run in a completely straight line as a function of gate voltage or from noise overlaying the peak structure of the diamonds, we determined the minimum and the maximum possible values for E_C and Δ that could be extracted when combining the peak positions of the CO for all cross sections. We found the values of E_C and Δ to vary by less than 4%. However, the change in these values as seen in Fig. 9 is more than a factor of 3 larger.

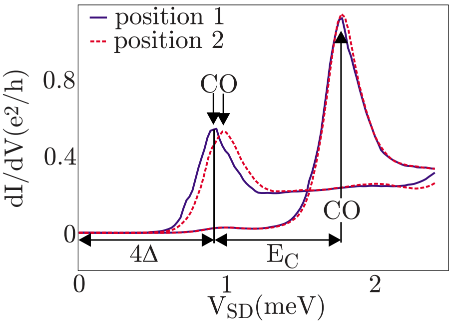

FIG. 10. (Color online) Cross sections of two different Coulomb diamonds. Each set of lines of the same color belongs to one Coulomb diamond. Arrows mark the positions of the current onset in each trace.

The correlation between E_C and Δ is highly unexpected. Since the SET is metallic, screening should occur on the surface within the first Angstroms of the sample. Furthermore the junctions are buried and should not be subjected to the influence of the tip. The superconducting properties of the system have their origin in the volume of the system and not on the surface and should therefore not be influenced by the SFM tip.

VIII. NUMERICAL SIMULATIONS

In order to gain further knowledge about the electrostatics of the complete system (sample and SFM tip) and therefore learn more about the behavior of the capacitances, simulations are carried out with the software tool COMSOL. The geometry is modeled following the SEM pictures of the structure (Fig. 1). The tip is approximated as a cone, i.e., having a round cross section closed to the sample with a diameter of 40 nm, which increases when moving further away from the structure. The tip is positioned at different positions with respect to the island and the electric field is calculated. Furthermore the capacitances of the tip, gate source, and drain are determined with respect to the island.

Figure 11 shows the magnitude of the electric field in color, whereas the sample outline is marked by the black lines. The apex of the tip is depicted by the black circle. Figure 11(a) shows the electric field when the tip is positioned precisely above the island. The sample geometry is approximately mirror symmetric left to right. This is reflected by the electric field distribution, which is also symmetric. When moving the tip away from this symmetry axis toward the left above one lead, the electric field ceases to be symmetric. Rather a high electric field is now found in the vicinity of the tip around the left lead. The electric field can be influenced by the position [Figs. 11(a) and 11(b)] and voltage (not shown) applied to the tip. Moving the tip over source or drain leads to an asymmetric electric field with respect to the sample symmetry axis.

Although the shape of the tip in our simulations has been simplified compared to the experimental setup, the capacitances obtained from the simulation show very good agreement with the experimental values. All numbers are within a factor of 2 of the measured values and their relative magni-

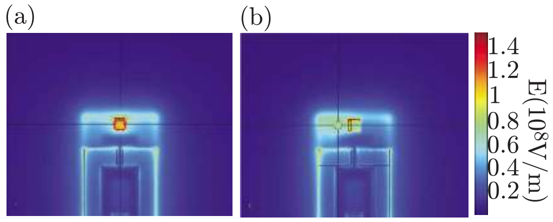

(c)

	Cs(aF)	CG(aF)	CD(aF)	CT(aF)	CI(aF)
A	-119	-0.08	-119	-2	243
B	-120	-0.11	-120	-1	242
C	80	0.2-0.28	80	0.4-1.2	

FIG. 11. (Color online) [(a) and (b)] Magnitude of the electric field in 10^8 V/m as obtained from simulations carried out with COMSOL. For (a) the tip is positioned above the SET as indicated by the black circle, whereas for (b) the tip is above the left lead (source). (c) Capacitances with respect to the island obtained from the simulation. The abbreviation S stands for source, D for the right lead (drain), I for island, G for gate, and T for the tip. Row A shows the values corresponding to the situations shown in plot (a), whereas row B corresponds to figure (b). Numbers in row C are values obtained from the experimental data.

tudes match the experimental data [see table in Fig. 11(c)]. The relative change of those values obtained from the simulations also agrees with the experimental data. Experimentally the gate capacitance C_G decreases by about 50% when placing the tip between the gate and the island as can be seen in Fig. 7; a change that is also seen in the simulations. The tip-island capacitance C_T can also be seen to decrease when the tip is moved away from the island in good agreement with experimental data. The capacitances of the junctions (C_S, C_D), however, remain unchanged when the tip is placed in different positions.

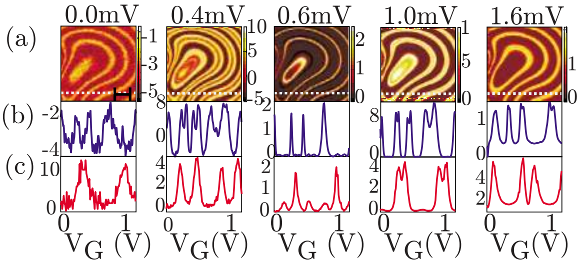

FIG. 12. (Color online) Scanning gate measurements for different V_{SD} values, as indicated on the top of each column. The top row (a) shows the scanning gate image. Color bars show the differential conductance in dI/dV_{SD} in 10^{-4} e^2/h for the first two columns, in units of 10^{-2} e^2/h for the second and third, and in units of 10^{-1} e^2/h for the fifth column. The scale bar has a length of 200 nm. Row (b) shows a cross section through this image at the position of the gray dashed line in the scanning gate image. The y axis shows the differential conductance in dI/dV_{SD} in the same units as the color bar of the scanning gate plot above. Row (c) shows the corresponding cut through the Coulomb diamond. The y axis shows dI/dV_{SD} in units of 10^{-3} e^2/h for the first, 10^{-2} e^2/h for the second, 10^{-1} e^2/h for the third, and e^2/h for the last two columns. Overall a good agreement between the images in rows (b) and (c) is reached. However, some of them differ in some fine structures. The tip-sample distance is around 50 nm, T=700 mK, V_{gate}=0 V, and B=0 T

IX. CONCLUSION

We have presented scanning gate measurements on a superconducting SET. Excellent correlation between scanning gate measurements and charge stability measurements is observed. Small differences remain. This leads to the conclusion that the in-plane gate has a slightly different effect on the SET than the movable out-of-plane gate: the period of the Coulomb blockade peaks can be influenced by the lateral position of the SFM tip. The tip potential consists of two parts; only one of which depends on the voltage applied to it. This supports the findings in Ref. 13. We furthermore observe an anticorrelation between the gate capacitance and the tip capacitance, which can be explained in terms of the screening the tip exerts. The exact origin of the observed and surprising anticorrelation between the charging energy and the superconducting gap cannot be explained by the electric field configuration of the setup which has been simulated considering the geometry of the tip and the device.

ACKNOWLEDGMENTS

We would like to especially thank René Monnier and Wolfgang Belzig for many fruitful discussions. We acknowledge financial support by ETH Zurich and the NCCR Nanoscale Science of the Swiss National Science Foundation,

APPENDIX: SCANNING GATE MEASUREMENTS IN DEPENDENCE OF V_{SD}

The influence of the source-drain voltage on the scanning gate measurements is investigated in another series of measurements, parts of which are shown in Fig. 12. Row (a) shows the scanning gate measurement taken at a distance z =50 nm of the tip above the surface, T=700 mK, V_G =0 V, B=0 T, and the indicated source-drain voltage. We observe that the shape of the rings always stays the same. However, the shape and number of peaks shown in the cross sections in row (b) are altered by V_{SD}. The measurement taken at V_{SD}=0 V shows small single peaks with approximately equal spacing. The measurement taken at V_{SD} =0.4 mV shows double peaks. The other measurements show again different peak structures. In order to make the peak structures more easily visible a cross section through those scanning gate images at the position of the gray dashed line is shown in row (b).

When looking at the Coulomb blockade diamond in Fig. 2(d) one can see that for cross sections at different V_{SD} values different peak structures have to be expected. In order to make these peak structures more easily tangible the cross sections through the Coulomb diamonds are shown in Fig. 12(c). We see that for different V_{SD} the differential conductances vs V_G traces show different peak structures.

Because our SFM tip acts as a movable gate, changing the voltage on the tip should have a similar effect as changing the voltage applied to the in-plane gate. Therefore the cross-section peak structures of the Coulomb diamonds should also be observable in the corresponding scanning gate images [Fig. 12 row (a)].

When comparing row (b) to row (c) in Fig. 12 we notice a good correlation between those two sets of measurements with respect to peak shape, height, and spacing. Notably the measurements for $V_{SD}=0,0.6,1.0$ mV show an almost perfect consistency. The correlation seems not quite as good for the measurements with $V_{SD}=0.4,1.6$ mV. For $V_{SD}=0.4$ mV the scanning gate measurement shows just barely split double peaks, whereas the cross section taken from the Coulomb diamond shows double peaks but with minima between them that have all the same depth. For $V_{SD}=1.6$ mV the scanning gate image shows the beginning of a peak splitting into double peaks, where we would expect clean single peaks from the Coulomb diamond measurement.

---

*huefner@phys.ethz.ch

[1] L. P. Kouwenhoven, D. G. Austing, and S. Tarucha, Rep. Prog. Phys. **64**, 701 (2001).

[2] A. T. Johnson, L. P. Kouwenhoven, W. de Jong, N. C. van der Vaart, C. J. P. M. Harmans, and C. T. Foxon, Phys. Rev. Lett. **69**, 1592 (1992).

[3] S. H. Tessmer, P. I. Glicofridis, R. C. Ashoori, L. S. Levitov, and M. R. Melloch, Nature (London) **392**, 51 (1998).

[4] M. A. Topinka, B. J. LeRoy, R. M. Westervelt, S. E. J. Shaw, R. Fleischmann, E. J. Heller, K. D. Maranowski, and A. C. Gossard, Nature (London) **410**, 183 (2001).

[5] G. A. Steele, R. C. Ashoori, L. N. Pfeiffer, and K. W. West, Phys. Rev. Lett. **95**, 136804 (2005).

[6] R. Crook, J. Prance, K. J. Thomas, S. J. Chorley, I. Farrer, D. A. Ritchie, M. Pepper, and C. G. Smith, Science **312**, 1359 (2006).

[7] A. Baumgartner, T. Ihn, K. Ensslin, G. Papp, F. Peeters, K. Maranowski, and A. C. Gossard, Phys. Rev. B **74**, 165426 (2006).

[8] C. R. da Cunha, N. Aoki, T. Morimoto, Y. Ochiai, R. Akis, and D. K. Ferry, Appl. Phys. Lett. **89**, 242109 (2006).

[9] A. Pioda, S. Kicin, T. Ihn, M. Sigrist, A. Fuhrer, K. Ensslin, A. Weichselbaum, S. E. Ulloa, M. Reinwald, and W. Wegscheider, AIP Conf. Proc. **772**, 781 (2005).

[10] S. Kicin, A. Pioda, T. Ihn, M. Sigrist, A. Fuhrer, K. Ensslin, M. Reinwald, and W. Wegscheider, New J. Phys. **7**, 185 (2005).

[11] A. Pioda, S. Kicin, T. Ihn, M. Sigrist, A. Fuhrer, K. Ensslin, A. Weichselbaum, S. E. Ulloa, M. Reinwald, and W. Wegscheider, Phys. Rev. Lett. **93**, 216801 (2004).

[12] P. Fallahi, A. C. Bleszynski, R. M. Westervelt, J. Huang, J. D. Walls, E. J. Heller, M. Hanson, and A. C. Gossard, Nano Lett. **5**, 223 (2005).

[13] A. E. Gildemeister, T. Ihn, M. Sigrist, K. Ensslin, D. C. Driscoll, and A. C. Gossard, Phys. Rev. B **75**, 195338 (2007).

[14] A. E. Gildemeister, T. Ihn, R. Schleser, K. Ensslin, D. C. Driscoll, and A. C. Gossard, J. Appl. Phys. **102**, 083703 (2007).

[15] M. Furlan, T. Heinzel, B. Jeanneret, S. V. Lotkhov, and K. Ensslin, Europhys. Lett. **49**, 369 (2000).

[16] G. J. Dolan, Appl. Phys. Lett. **31**, 337 (1977).

[17] E. H. Visscher, S. M. Verbrugh, J. Lindeman, P. Hadley, and J. E. Mooij, Appl. Phys. Lett. **66**, 305 (1995).

[18] T. Ihn, *Electronic Quantum Transport in Mesoscopic Semiconductor Structures*, Springer Tracts in Modern Physics 192 (Springer, New York, 2004).

[19] A. Maassen van den Brink, G. Schön, and L. J. Geerligs, Phys. Rev. Lett. **67**, 3030 (1991).

[20] T. A. Fulton and G. J. Dolan, Phys. Rev. Lett. **59**, 109 (1987).

[21] R. J. Fitzgerald, S. L. Pohlen, and M. Tinkham, Phys. Rev. B **57**, R11073 (1998).

[22] D. V. Averin, A. N. Korotkov, A. J. Manninen, and J. P. Pekola, Phys. Rev. Lett. **78**, 4821 (1997).

[23] J. F. Cochran and D. E. Mapother, Phys. Rev. **111**, 132 (1958).

[24] T. A. Fulton, P. L. Gammel, D. J. Bishop, L. N. Dunkleberger, and G. J. Dolan, Phys. Rev. Lett. **63**, 1307 (1989).

[25] P. Hadley, E. Delvigne, E. H. Visscher, S. Lahteenmaki, and J. E. Mooij, Phys. Rev. B **58**, 15317 (1998).

[26] A. E. Gildemeister, T. Ihn, M. Sigrist, K. Ensslin, D. C. Driscoll, and A. C. Gossard, Appl. Phys. Lett. **90**, 213113 (2007).

[27] A. Pioda, S. Kicin, D. Brunner, T. Ihn, M. Sigrist, K. Ensslin, M. Reinwald, and W. Wegscheider, Phys. Rev. B **75**, 045433 (2007).